REVIEW OF SCIENTIFIC INSTRUMENTS **89**, 053904 (2018)

Self-contained in-vacuum *in situ* thin film stress measurement tool

J. Reinink, R. W. E. van de Kruijs, and F. Bijkerk
Industrial Focus Group XUV Optics, MESA+ Institute for Nanotechnology, University of Twente, Drienerlolaan 5, 7522NB Enschede, The Netherlands

(Received 8 January 2018; accepted 23 April 2018; published online 14 May 2018)

A fully self-contained in-vacuum device for measuring thin film stress *in situ* is presented. The stress was measured by measuring the curvature of a cantilever on which the thin film was deposited. For this, a dual beam laser deflectometer was used. All optics and electronics needed to perform the measurement are placed inside a vacuum-compatible vessel with the form factor of the substrate holders of the deposition system used. The stand-alone nature of the setup allows the vessel to be moved inside a deposition system independently of optical or electronic feedthroughs while measuring continuously. A Mo/Si multilayer structure was analyzed to evaluate the performance of the setup. A radius of curvature resolution of 270 km was achieved. This allows small details of the stress development to be resolved, such as the interlayer formation between the layers and the amorphous-to-crystalline transition of the molybdenum which occurs at around 2 nm. The setup communicates with an external computer via a Wi-Fi connection. This wireless connection allows remote control over the acquisition and the live feedback of the measured stress. In principle, the vessel can act as a general metrology platform and add measurement capabilities to deposition setups with no modification to the deposition system. © *2018 Author(s). All article content, except where otherwise noted, is licensed under a Creative Commons Attribution (CC BY) license (http://creativecommons.org/licenses/by/4.0/).*
https://doi.org/10.1063/1.5021790

I. INTRODUCTION

The physics of thin film deposition is an active research area with many properties remaining to be characterized. One important property is the intrinsic stress. Various macroscopic properties, such as electrical conductivity,[1] optical response,[2] and mechanical quality,[3] all depend on the stresses that develop during thin film manufacturing. Among the mechanical failure mechanisms, strong compressive stress can lead to delamination, whereas strong tensile stress can lead to cracking. Therefore, stress engineering is important for many applications such as hard coatings on machining tools,[4] solar cells,[5] micro electronics,[6] and multilayered coatings for EUV optics.[7]

In situ measurement methods can offer a wealth of information on the development of the layer during deposition. Thin film stress is directly related to the layer structure and composition, and measuring the development of stress during growth can provide information about layer growth properties such as island growth,[8] compound formation,[9] and crystallization.[10] In general, optical measurement techniques are favored over electrical methods such as capacitive deflection measurements because laser beams experience no interference from the plasma used in many deposition processes.[11] This makes the setup usable in all PVD processes. CVD processes are not directional and also coat the backside of the cantilever, resulting in no curvature change as well as coating the optical windows of the measurement beams.

Most of the optical *in situ* stress measurement setups are based on the use of a light path that starts and ends outside the deposition chamber and as such require a line of sight to the substrate,[12–15] which is generally stationary during the measurements. However, many coaters rotate the substrate to increase the uniformity of the deposited layer. Optical measurement techniques can be triggered by the rotation of the substrate[16–18] to enable measurements, but this limits the measurement rate to the rotation frequency and requires short integration times where long integration times are preferable for averaging out vibrations. A further complication arises when the substrate moves through the chamber in a planetary motion. To our knowledge, there is currently no *in situ* stress metrology tool available that can function in such an environment.

In this work, we present an optical *in situ* stress measurement setup capable of working in a vacuum deposition chamber where the substrate can make any type of motion. This was done by integrating all measurement optics and electronics in a vacuum compatible vessel that remains at atmospheric pressure. Due to its stand-alone nature, the setup requires no electrical connection or optical feedthroughs and can operate fully isolated. This eliminates the need for extensive infrastructure to enable the measurements, and the setup can be integrated into existing deposition systems without their modification. The curvature of the cantilever sample was determined by measuring the deflection of two lasers beams off the cantilever, which by using Stoney's equation was converted to a stress value. We discuss the vacuum and mechanical aspects, the design of the laser deflectometer, the electronics, the influences of the environment inside a deposition system, and the Wi-Fi communication implemented. This is followed by several demonstration stress measurements performed using the setup. The stand-alone nature of the measurement setup makes it an ideal platform to integrate many more measurement capabilities into that might otherwise not be available in

 © Author(s) 2018

a deposition system, such as a Faraday cup, a Langmuir probe, or a quartz mass balance.

II. DESIGN OF THE *IN SITU* STRESS MEASUREMENT SETUP

The design of the *in situ* stress measurement setup covers several aspects: vacuum technology, optical measurements, communication, and environmental conditions.

A. Vacuum and mechanical

The setup was designed in the form factor of a substrate holder of a Roth & Rau MS1600 deposition system (see Fig. 1). Achieving compatibility with the deposition system also imposed a weight limit of 20 kg. During the thin film deposition process, the substrate was sequentially moved over the stationary magnetrons for deposition of each layer while the substrate was rotating along its own axis to ensure homogeneous deposition over a large substrate area. The internal space available is approximately 25 cm in diameter and 15 cm high and houses the electronics and optics.

The vacuum vessel shields the vacuum of the process chamber from those components that are not vacuum compatible and provides a suitable atmosphere for electronic components that can only function at atmospheric pressure. The vessel itself was made of aluminum and sealed with Viton o-rings. Filling the vessel with helium and introducing it into the process chamber showed no increase in He in the RGA spectrum, indicating a negligible leak rate.

The vessel has several feedthroughs. At the bottom are two windows situated behind the cantilever to pass the optical beams out and into the vessel. At the side four feedthroughs are available. One was used for the Wi-Fi antenna. The option to add a second antenna at the other side of the vessel existed but the connection was already stable with only one. The other feedthroughs can be used for other purposes; for example, passing a thermocouple for external temperature measurements or to allow charging of the batteries without opening the vessel.

B. Optical

1. Setup/component choice

The curvature of the cantilever sample is proportional to the intrinsic stress of the deposited layer. Detection of the cantilever curvature was achieved by deflecting two laser beams off the cantilever and measuring their position using a camera after a certain propagation length. The difference in deflection is proportional to the curvature of the sample in between the beams. The beam near the clamp has little deflection and is therefore used as reference for the beam at the end of the cantilever. The optical system is shown in Fig. 2. Using only two beams allows for a simple optical design and allows for the tilt of the whole cantilever, for example, by thermal expansion effects in the clamp, to be canceled out by measuring the position of the beams relative to each other.[19] The cantilevers used are cut from ⟨100⟩ Si wafers and are 25×90 mm in size. Clamping the cantilever at only one end allows free bending of the whole cantilever.

A fiber-coupled diode laser was chosen for its high beam quality, small size, simplicity, and low power consumption. The laser was set for a low operating power to accommodate the increasing operating current in response to the increasing temperature. The fiber ends in a collimator mounted on the breadboard. The collimator was adjusted to give a slightly converging beam to achieve a small spot size on the camera. The beam was sent via mirror M1 to the beamsplitter (BS) to generate two beams.

The beam path between splitting and combining the beams has equal path lengths to ensure equal sensitivity to cantilever bending. Mirrors M2, M3, and M4 are folding mirrors that bring the beams from the beamsplitter to both ends of the cantilever. A large beam separation of 60 mm was used to achieve a high sensitivity. By using a beamsplitter to both split and combine the beams, the two beam paths fall on the same camera while having a large separation at the sample. One of the beams was given an out-of-plane offset to prevent overlapping of beams on the camera. Both beams can travel the full length across the camera sensor without encountering other beams, providing a wide measurement range.

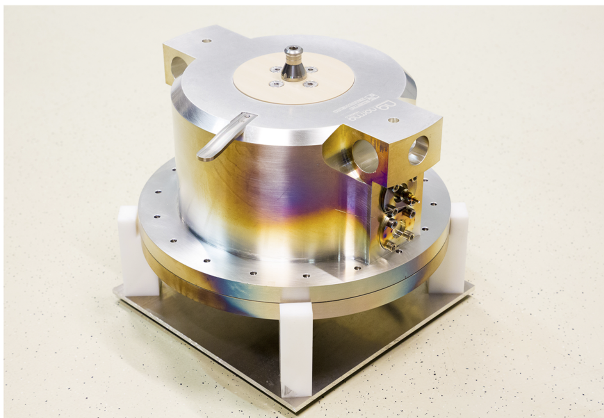

FIG. 1. The vessel placed on a stand, showing two of four 4 KF16 flanges on the sides. The two holes on the sides and the pin on top are for handling the vessel by a loading mechanism in the deposition system.

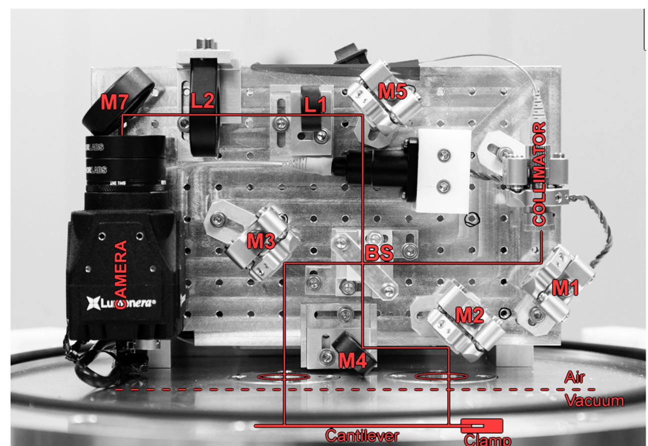

FIG. 2. Optical bench with the components marked. The cantilever was mounted beneath the baseplate (not visible in the photo). The breadboard is 18×11 cm and has a 12.5 mm pitch.

Mirror mounts M2 and M3 are Newport AG-M050N piezo-actuated mirror mounts (normal mounts are shown in Fig. 2). This allows remote control of the alignment of both beams when the setup is closed. The substrate must be a double-sided polished cantilever to allow the beams to be reflected off the backside. The substrate shields the two windows passing the beams in and out of the vessel from the deposition flux. A beam expander consisting of a −6 mm focal length lens (L1) and a 50 mm focal length lens (L2) was installed to increase the sensitivity of the setup. Scanning the beams across the beam expander using the piezo mirror mount shows excellent linearity with only ±0.5% deviation. The resulting 0.5% uncertainty was considered negligible.

A Lumenera Lt425M-WOCG camera was chosen for its large sensor width of 11.3 mm and the absence of the cover glass of the CMOS sensor, eliminating fringes normally present due to a coherent source. It can capture 90 fps at the 4 megapixel resolution, allowing very fast processes to be captured even at high deposition rates.

When the setup is opened, the breadboard and sample remain in place; this allows the setup to stay aligned when the vessel is opened and closed for maintenance or to exchange either batteries or storage media. The piezo mirror mounts allow realignment after the vessel is closed, which can be used for compensating the deformation of the vessel when cycling from atmosphere to vacuum and for realignment after changing samples without opening the vessel.

2. Measurement range and noise

The setup was designed to measure stress in multilayer systems such as a Mo/Si multilayer mirror. These typically have stress values of a several hundred MPa and a thickness of several hundred nanometers leading to a total force per unit width (F/w) of 100 N/m. Individual layers can have features in the stress development of 0.5 N/m occurring within 0.5 s. These features must be resolved from the noise.

The optical setup on the breadboard was made compact because of the limited available space. Due to this, the optical path from the cantilever to the camera is only 340 mm. The sensitivity was increased to the equivalent of a 2.1 m path length by using a beam expander. Propagation from the cantilever to the camera was calculated using ABCD matrices.

The measurement range using a 525 μm thick Si cantilever is 280 N/m with the beam staying in the center 75% width of the camera sensor to avoid clipping the beams, corresponding to a maximum radius of curvature of 30 m. The beams have a FWHM of 1.4 mm or 250 pixels at the camera. This range is sufficient to capture a full multilayer stack. There are several ways in which the range can be increased or decreased for other applications. Thinner wafers decrease the range, which is suited for measuring a single or several thin layers. Thicker wafers can be used for thicker layers or systems. Reducing or increasing the magnification of the beam expander increases or decreases the range, respectively.

The calculation of the sensitivity of the setup is only approximate as the path lengths have an uncertainty due to alignment. Calibration was performed by measuring the initial and final cantilever curvature *ex situ* using a white light interferometer and matching the *in situ* measurement result to the *ex situ* measured curvature change.

Vibrations present in the system, such as the substrate movement over the magnetrons, were the main source of noise in the measurements. Typical measurement parameters are a 10 Hz acquisition rate, an 80 ms integration time, and a 300 μm thick Si cantilever. The RMS noise measured for this configuration is 0.03 N/m. This is mostly due to oscillations present at much higher frequencies than the features in the stress development. A simple Gaussian moving average filter with a 1 Hz −3 dB point was found to be ideal to reduce noise while still resolving important features accurately. This filter effectively removes the noise that is due to the acceleration and deceleration of the substrate from magnetron to magnetron and reduces the noise to well below 0.01 N/m (shown in Fig. 7), corresponding to a 270 km radius of curvature.

The piezo mirror mounts can move the beam back onto the camera when the substrate curvature increases. This can extend the range to the point where Stoney's equation becomes non-linear. A 300 μm thick Si cantilever thickness was used in the measurements presented in this work, as this provided sufficiently low noise while having a large enough range to require few adjustments of the piezo mirror mounts.

C. Electronics

For the system to be fully standalone, all the electronics needed to perform the measurement must be inside the vessel. The system must operate for the full duration of the deposition, which can take up to 10 h for multilayers with over 200 periods, for example, as used for 6.7 nm radiation. The opened vessel is shown in Fig. 3. A low power single board computer is used to read out the camera in order to save space and power consumption. A Fitlet iA10 single board computer with the heatsink option was chosen as this computer is rated to operate at 60 °C and has a build-in Wi-Fi adapter. It runs Debian Linux for stability, versatility, and low overhead. The system is battery powered with two battery packs of total capacity 200 Wh. The measured power usage when idling was 10 W,

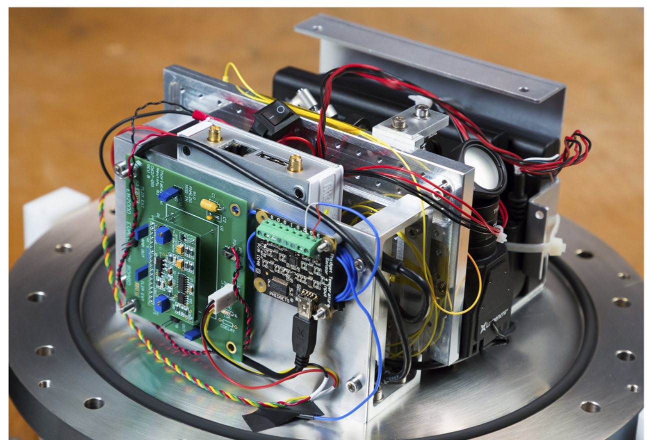

FIG. 3. An overview photo of the setup, showing (front to back) the laser diode driver and thermocouple card, the Fitlet computer, optical breadboard, and battery packs.

while at a 10 Hz acquisition rate the usage was 13 W. The achieved runtime is over 12 h, sufficient for the deposition of multilayers with over 200 periods.

D. Environment

1. Thermal

The only way for the setup to dissipate heat when in vacuum is by radiative heat transfer. Electronic components have limited operating temperatures, with the camera and laser diode being limited to 50 °C. This requires a low power dissipation in the setup to prevent overheating of the setup during a long deposition. The computer's central processing unit (CPU) and the camera are fitted with extra heat sinking to prevent the CPU from throttling and to lower the noise level of the camera's CMOS sensor. A 4-channel thermocouple universal serial bus (USB) card from Phidgets Inc is included to measure temperatures inside the vessel and prevent overheating.

The setup can be modeled by a simple thermal model,

$$dT/dt = \frac{P_e + P_{mag} - \epsilon\sigma A(T^4 - {T_{chamber}}^4)}{C}, \quad (1)$$

where the input power consists of the electronic power usage P_e and the heat input from the magnetrons is denoted as P_{mag}. ϵ is the emissivity of the outside of the vessel and A is the outside area; σ is the Stefan-Boltzmann constant; $T_{chamber}$ is the temperature of the process chamber; and T the temperature of the vessel. The heat capacity of the system is denoted as C.

The electronic power usage is estimated by measuring the current drawn from the batteries and multiplying it by the battery voltage. The area of the vessel is approximately 0.3 m^2. The heat input from the magnetrons, the emissivity, and the heat capacity are derived from fitting the model to the measured vessel temperature. The magnetron deposition process deposits 5 W on average when depositing a Mo/Si multilayer. Depositing a single period of a Mo/Si multilayer takes 167 s. The emissivity of the aluminum vessel is very low (around 0.15) and thus there is very little heat transfer by radiation. Due to its high heat capacity of 15 kJ/K, the temperature of the vessel increases slowly. The vessel reached around 50 °C at the end of the 12 h battery duration during which a 50 period Mo/Si multilayer was deposited.

Longer or higher power coatings require extra measures to prevent the operating temperature being exceeded. The temperature of the vessel, optical breadboard, computer heatsink, and camera heatsink is monitored to prevent overheating. Better cooling can be achieved by applying a high emissivity coating on the vessel. An emissivity of 0.25 would be sufficient for continuous coating of Mo/Si periods.

2. Vibrations

Mechanical vibrations were the main source of noise in the measurement. The long cantilever behaves like a tuning fork and is particularly sensitive to its eigenfrequency and the harmonics of that. Avoiding overlap between the vibrations present and the eigenfrequency is achieved by using a cantilever of a specific length. Combined with a long integration time that averages out vibrations, this resulted in a sufficiently low noise level.

Reducing the effect of vibrations can be improved by measuring the spectrum of the vibrations present. This allows choosing an optimum cantilever length. Choosing an integration period equal to a (sub)harmonic of the cantilever reduces the noise from oscillations of the cantilever. This was not done as the obtained noise performance was already more than adequate.

E. Communication

Control over the acquisition process and a realtime transfer of the measurement data allows verification of the performance of the setup and a realtime feedback loop of the deposition process. As the setup is fully self-contained, this requires wireless communication. A Wi-Fi connection was implemented to access the setup remotely and to transfer the camera images. An external computer performs the image processing to obtain the stress values and provides a live view of the stress development. This reduces the computation load of the setup but requires sufficient bandwidth to transfer the images. The setup continues independent of the external computer and saves the measurements locally in case the Wi-Fi connection or the external computer fails.

Both the vessel and the process chamber have an electrical feedthrough to which a short wire antenna was connected for the Wi-Fi communication. In case an electrical feedthrough is not available in the process chamber, placing the antenna in front of a viewport is also possible.[20] Both sides support the 802.11ac standard, giving a theoretical bandwidth of 433 Mbit/s. The connection was very reliable; a Wi-Fi connection could even be maintained in the sealed loadlock where no antenna was present. It is assumed that the viewport on the loadlock passes the signal in and out. The Wi-Fi connection was not influenced by the magnetron plasma from either the DC or the RF magnetrons. Substrate rotation of the whole setup at 1.5 Hz did not affect the connection either. Deposited material on the antenna did not noticeably affect the Wi-Fi performance.

Images of the full 4 megapixel resolution are approximately 200 kB after JPEG compression at a quality level of 90. This can increase to 270 kB as the system heats up and the camera noise level increases. A 1.5 MB/s download speed was obtained, transferring data from the setup to the Wi-Fi access point. However, this is only sufficient for an acquisition rate of 5 Hz.

An upload speed of 4.5 MB/s was achieved, demonstrating that sufficient bandwidth can be achieved. Proper antenna optimization and hardware choice should at least bring the download speed up to this level. The antenna length and geometry were not calculated or optimised, and this is most likely the reason for the low transfer rate. A 10 Hz rate was used in Fig. 5; this was captured locally as the realtime feedback was not needed for the experiments performed. For this reason, no bandwidth saving measures, such as specifying a region of interest in the camera to exclude unused parts of the image, were taken.

III. MEASUREMENTS

A. Acquisition

During measuring the stress, the camera continuously captures images and stores them in the JPEG format to conserve disk space and decrease the required bandwidth of the Wi-Fi connection. The acquired images are stored on a USB mass storage device connected to the Fitlet computer and are accessible via the Wi-Fi connection. The in-house written software has an 18 ms dead time per image. This leads to a maximum acquisition rate of 50 Hz. As this is already sufficient to obtain sub-monolayer resolution for deposition rates of several nanometers per second, this was not further optimised. The deposition speeds used in this work are around 0.2 nm/s, making a 50 Hz rate unnecessary. A 10 Hz acquisition rate at a 80 ms integration time was chosen for most measurements, which still provides sub-monolayer resolution as well as a low noise due to the long integration time.

B. Processing

The live view calculated on the external computer calculates the center of mass of the beam profile on the images to determine their position. In addition, the full measurement data were processed after the measurement was finished using a 2D Gaussian fitting to determine the positions of the beam profiles more accurately. This calculation is not fast enough to be used for the live view in the current software implementation.

The beam position on the camera corresponds to the curvature. Stoney's equation, as shown in (2), is used to convert the curvature to the force per unit width,

$$\sigma h = \frac{E_s h_s^2}{6(1-\nu)}(\kappa - \kappa_0). \tag{2}$$

E_s and ν are Young's modulus and Poisson ratio, respectively, of the substrate, h is the coating thickness, and h_s is the thickness of the cantilever used. For Stoney's equation to be linear, $h \ll h_s$ must be valid. The initial curvature κ_0 is subtracted from the curvature κ to remove any effect of the substrate curvature. σ is the coating stress.

The force per unit width (F/w) is defined as σh and is directly proportional to the measured curvature. The derivative of the force per unit width is the incremental growth stress expressed in N/m^2 and shows the stress of the newly added material but also includes any stress changes induced in the substrate layer by the added material. A linear stress development in a F/w curve during layer growth therefore indicates a material growth at constant stress. However, since numerical derivation introduces high noise levels, F/w is used in this work.

C. Example measurements

To evaluate the performance of the metrology setup, *in situ* stress measurements were carried out during the deposition of a Mo/Si multilayer. The growth of Mo/Si is well characterized in the literature, and pioneering experiments on *in situ* stress have been reported,[21] although those measurements were carried out without substrate movement or rotation.

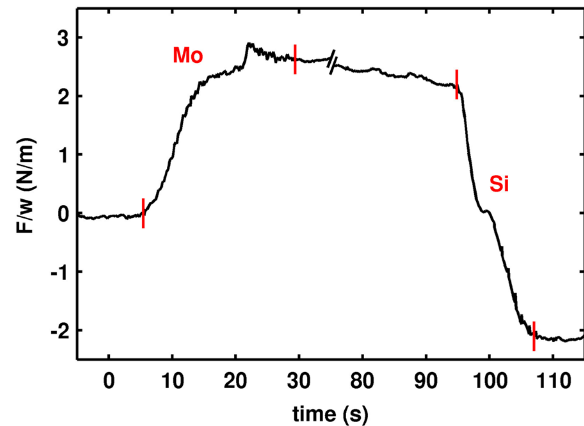

FIG. 4. Force per unit width recorded during a single period of a Mo/Si multilayer. This measurement has a 5 Hz acquisition rate at a 100 ms integration time.

In Fig. 4, the force per unit width recorded during a single period of a Mo/Si multilayer is shown. The as-deposited thicknesses are 3.5 nm for Mo and 4.5 nm for Si, typical for applications of these multilayers in EUV imaging applications.

The stress development of the coating reveals several interesting features. At 20 s, there is a tensile jump in the Mo stress after which the growth has changed from tensile to compressive. This is the transition from the amorphous phase to the polycrystalline phase which is known to occur around 2 nm.[22,23] The Si stress development shows a very small tensile peak at 100 s. This is attributed to the end of the molybdenum silicide interlayer formation and the start of pure Si growth.[9,24]

As discussed in Sec. II B 2, by using the piezo-actuated mirror mounts, a wide measurement range can be achieved. To evaluate the operation of the metrology device over many periods, a 250 period Mo/Si multilayer was deposited and the *in situ* stress measurements are shown in Figs. 5–7. The results show a near constant stress per period over the full 250 period range. A linear fit to the data shows a quadratic residue with a ±1% deviation, which may be due to the non-linearity of Stoney's equation becoming significant as the total coating

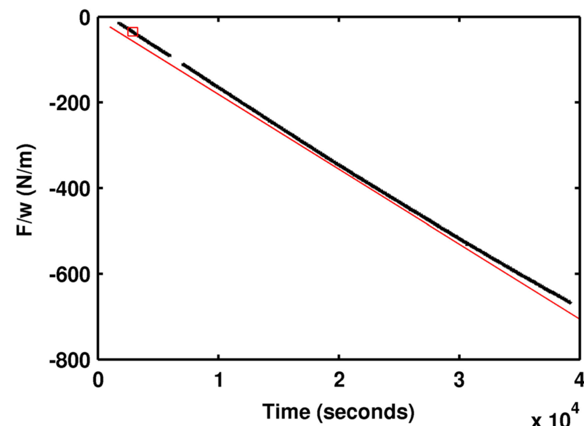

FIG. 5. F/w of a 250 period MoSi deposition including a linear fit. The linear fit has an offset to avoid obscuring the data. The gap at 6000 s is an interruption in the data acquisition.

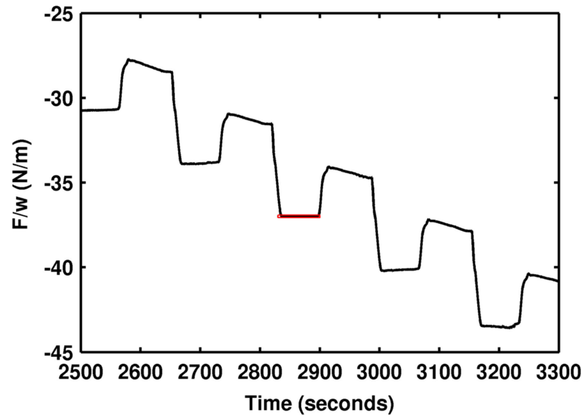

FIG. 6. Magnification of indicated area of Fig. 5 showing 4 Mo/Si periods.

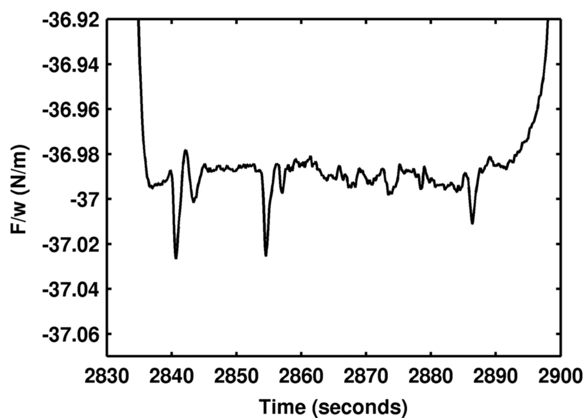

FIG. 7. Magnification of indicated area of Fig. 6 showing a 0.01 N/m noise level after a 1 Hz moving average filter was applied.

thickness is 1.75 μm on a 300 μm thick cantilever. In addition, roughening of the multilayer can also influence growth in the tensile direction.

The heat input from the magnetrons also heats the substrate, typically by 1–2 °C after a single layer, leveling off to 10 °C during the normal deposition process. For thin coatings, the cantilever can expand and contract without affecting the curvature. For thick coatings, the unequal thermal expansion of the cantilever and coating induces a curvature change. The resulting curvature change can be modeled and subtracted if needed.

IV. CONCLUSIONS

We have developed a self-contained in-vacuum *in situ* stress measurement setup which was mounted in a substrate holder in a UHV deposition system, while electrically and optically fully isolated from the deposition system. The stress setup was tested to be capable of measuring the thin film stress development during deposition at a 0.01 N/m RMS noise level. This sensitivity was more than sufficient to reveal small layer growth features in the stress development such as the phase transformation of molybdenum from amorphous to polycrystalline. A live view of the stress development was implemented to monitor the stress realtime. The communication was achieved via a Wi-Fi connection.

The setup could, in principle, serve as a general in-vacuum metrology platform. Extended measurement options such as a Faraday cup can be integrated as well as features such as sample heating or sample bias, which are generally challenging to implement for a substrate that moves and rotates in a vacuum chamber. The stand-alone nature of the system allows the integration of an extensive platform for metrology or sample interaction without extensive modification of the deposition chamber.

ACKNOWLEDGMENTS

We acknowledge the support of the Industrial Focus Group XUV Optics at the MESA+ Institute for Nanotechnology at the University of Twente, notably the industrial partners ASML, Carl Zeiss SMT, and Malvern Panalytical, as well as the Province of Overijssel and the Foundation FOM (now part of the NWO, the Netherlands Organisation for Scientific Research).

[1] A. Steegen and K. Maex, Mater. Sci. Eng., R **38**, 1 (2002).
[2] R. Kumar, N. Khare, V. Kumar, and G. Bhalla, Appl. Surf. Sci. **254**, 6509 (2008).
[3] P. Mayrhofer, C. Mitterer, L. Hultman, and H. Clemens, Prog. Mater. Sci. **51**, 1032 (2006).
[4] T. Göbel, S. Menzel, M. Hecker, W. Brückner, K. Wetzig, and C. Genzel, Surf. Coat. Technol. **142-144**, 861 (2001).
[5] D. Antartis and I. Chasiotis, Sol. Energy **105**, 694 (2014).
[6] A. Özçelik, C. Van Bockstael, C. Detavernier, and R. Vanmeirhaeghe, AIP Conf. Proc. **899**, 453 (2007).
[7] M. Shiraishi, W. Ishiyama, T. Oshino, and K. Murakami, Jpn. J. Appl. Phys., Part 1 **39**, 6810 (2000).
[8] J. Floro, E. Chason, R. Cammarata, and D. Srolovitz, MRS Bull. **27**, 19 (2002).
[9] A. Yakshin, E. Louis, P. Görts, E. Maas, and F. Bijkerk, Phys. B **283**, 143 (2000).
[10] B. Krause, G. Abadias, A. Michel, P. Wochner, S. Ibrahimkutty, and T. Baumbach, ACS Appl. Mater. Interfaces **8**, 34888 (2016).
[11] M. Shiraishi, W. Ishiyama, N. Kandaka, T. Oshino, and K. Murakami, Proc. SPIE **4343**, 590 (2001).
[12] M. Bicker, U. von Hülsen, U. Laudahn, A. Pundt, and U. Geyer, Rev. Sci. Instrum. **69**, 460 (1998).
[13] J. Premper, D. Sander, and J. Kirschner, Rev. Sci. Instrum. **86**, 033902 (2015).
[14] A. Krost, A. Dadgar, F. Schulze, J. Bläsing, G. Strassburger, R. Clos, A. Diez, P. Veit, T. Hempel, and J. Christen, in *Proceedings of the 14th International Conference on Crystal Growth and the 12th International Conference on Vapor Growth and Epitaxy* [J. Cryst. Growth **275**, 209 (2005)].
[15] R. J. Drese and M. Wuttig, J. Appl. Phys. **98**, 073514 (2005).
[16] G. Abadias, L. Koutsokeras, P. Patsalas, W. Leroy, D. Depla, S. Zlotski, and V. Uglov, "*In situ* stress evolution during growth of transition metal nitride films and nanocomposites," in *Nanomaterials: Application and Properties* (Sumy State University, 2011), pp. 355–364, available at https://nap.sumdu.edu.ua/data/NAP-2011_Proc_Vol_1_Part_II.pdf (accessed 4 May 2018).
[17] S. Michotte and J. Proost, Sol. Energy Mater. Sol. Cells **98**, 253 (2012).
[18] See https://www.k-space.com/wp-content/uploads/MOS_Product_Specs.pdf for "k-space associates, inc" (accessed October 26, 2017).
[19] K. Dahmen, S. Lehwald, and H. Ibach, Surf. Sci. **446**, 161 (2000).
[20] A. Murari and L. Lotto, Vacuum **72**, 149 (2003).
[21] J. M. Freitag and B. M. Clemens, Appl. Phys. Lett. **73**, 43 (1998).
[22] S. Bajt, D. G. Stearns, and P. A. Kearney, J. Appl. Phys. **90**, 1017 (2001).
[23] E. Schubert, S. Mändl, H. Neumann, and B. Rauschenbach, Appl. Phys. A **80**, 47 (2005).
[24] E. Zoethout, E. Louis, and F. Bijkerk, J. Appl. Phys. **120**, 115303 (2016).